Research Papers

ISSN 2610-931X

CEIS Tor Vergata

RESEARCH PAPER SERIES

Vol. 23, Issue 8, No. 613 – October 2025

Modeling Euro Area Benchmark Rates After the End of LIBOR

Flavio Angelini, Stefano Herzel, Marco Nicolosi

Modeling Euro Area Benchmark Rates After the End of LIBOR

Flavio Angelini[*], Stefano Herzel[†], Marco Nicolosi[‡]

October 7, 2025

Abstract

We adopt an affine short-rate model for the contemporaneous evolution of the term structures based on EURIBOR and on €STR. The model is based on the observation that the risk-free rate follows a constant trajectory and moves only at deterministic times (depending on the European Central Bank meetings). We calibrate the model using Kalman filtering on a panel of term structure zero rates and compare its performances to the dynamic version of the Nelson-Siegel model, both in- and out-of-sample. The model is able to reproduce some common features of the term structure dynamics, such as the "snake" shaped term structure volatility and the fact that the volatility increases in periods containing the meeting dates. We analyze the sensitivity of the €STR term structure to variations in monetary policy expectations and apply the model to estimate the level and the probability distribution of the future rates, and to show how to compute the fallback risk of a on-going contract in case EURIBOR would be replaced by €STR.

Keywords: Affine Short-Rate Models, Bond Yields, Deterministic Jump Times, Fallback Risk, €STR Transition

JEL codes: C5, C6, E4, E5

[*]University of Perugia. E-mail: `flavio.angelini@unipg.it`
[†]Tor Vergata University of Rome. E-mail: `stefano.herzel@uniroma2.it`
[‡]Sapienza University of Rome. E-mail: `marco.nicolosi@uniroma1.it`

1 Introduction

In the recent years, several Risk-Free Rates (RFRs) have been proposed as the new benchmarks to replace the LIBOR rates. In the Euro Area, we assist to the coexistence of two indexes, the Euro Short-Term Rate (€STR) and the EURIBOR, with their respective term structures. The object of this paper is to propose a model for the study of these term structures.

The €STR is a rate which reflects the wholesale euro unsecured overnight borrowing costs in Euro zone. It is published for each business day based on transactions conducted and settled on the previous day (reporting date T) with a maturity date of $T + 1$ and which are deemed to be executed at arm length and thereby reflect market rates in an unbiased way. It was published for the first time on October 2, 2019 when it became the reference short-term risk-free rate for the Eurozone, replacing the EONIA rate which was finally dismissed on January 3, 2022. From Figure 1 we see that €STR closely follows the Deposit Facility rate (DFR), which is the rate settled by the European Central Bank (ECB) to remunerate the overnight deposits of the most important banks in the Euro area. The vertical lines represent the dates of the ECB meetings when the decisions on the monetary policy are taken. We see that €STR has been constantly below the DFR by a few basis points. This apparent arbitrage opportunity may be justified by market segmentation, as is documented in ECB (2025); in fact, the access to the Deposit Facility is not allowed to non-bank financial institutions, who lend their liquidity at rates lower than the DFR.

EURIBOR is an index calculated by the European Money Market Institute (EMMI) for five maturities (one week, and one, three, six and twelve months) and related to the rate at which euro wholesale funds could be obtained by credit institutions in current and former European Union and European Free Trade Association countries in the unsecured money market. The volumes of exchanges used in the determination of EURIBOR in the month of December 2024 was 145.5 billion for the 1 week maturity and much less (from 10.9 to 5.6 billion) for the other maturities (the data are accessible through the EURIBOR Transparency Indicator by the EMMI). As a comparison, transactions indexed to the €STR amounted to around €50 billion per day during the same month. It is important to note that the number of banks contributing to €STR is significantly higher than the number of banks contributing to EURIBOR. In fact, the set of EURIBOR banks is a subset, with a few exceptions, of the €STR set. Despite these facts that may highlight some issues in its representativeness, EURIBOR is still widely used as a reference for derivatives in the Euro money market. According to EMMI, at the end of 2024, the total outstanding amount of financial instruments and contracts using EURIBOR as a reference exceeded 100 trillion. However, the volume of futures contracts written on €STR is increasing and the working group on Euro RFRs provided several recommendation to include in financial contracts referring to EURIBOR also the indication of a fallback rate, in case of a future dismissal of EURIBOR, based on €STR ECB (2021).

For an appropriate comparison between EURIBOR and €STR we consider a term version of €STR extracted from Overnight Interest rate Swaps (OIS) written on €STR. Figure 2 shows that the spread between the 3 months EURIBOR and the corresponding OIS on €STR has almost always been positive in the period from 2019 to 2024. The spread is due to credit and liquidity risks that are present in the loans used to compute the EURIBOR but are negligible in

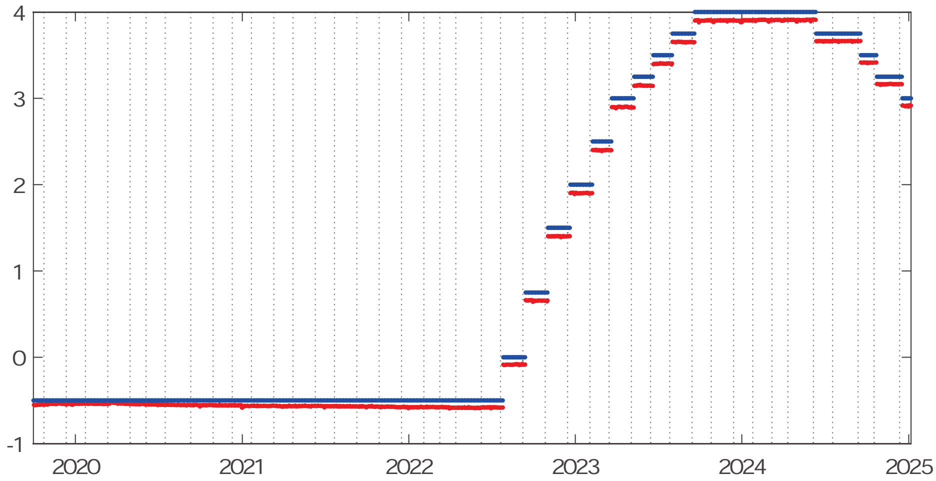

Figure 1: €STR (red line) and ECB Deposit Facility rate (blue line) from October 2020 to January 2025. The vertical dotted lines correspond to the dates of the meetings of the Board of ECB.

the OIS contracts (thanks to collateralization). EURIBOR reflects the credit risk of the banking sector, increasing in periods of market turmoils, while €STR often does the opposite, due to an effect of flight to quality. For this reason, the spread increased significantly, growing up to about 45 basis points, in 2020 during the pandemic and then decreased as the liquidity risk was at the lowest level due to the Quantitative Easing policy implemented by the ECB. Afterwards, when the ECB began raising the DFR, the volatility of the spread increased. We also note that it became negative for a relatively short period at the beginning of 2023, hitting a minimum level of about -20 basis points, possibly because of the excess of liquidity in the Euro money market. The spread turned positive and also became more volatile in March 2023, when global fixed income markets were hit by the collapse of Silicon Valley Banks in the United States and by the crisis at Credit Suisse in Switzerland, sparking fears of instability across the banking sector also in the Euro Zone, so that the one-year EURIBOR/€STR spread spiked at 70 basis points ECB (2025).

We propose a model where the €STR curve is driven by a latent short rate, which evolves as a continuous-time pure jump process, with jumps occurring only at deterministic times, corresponding to scheduled ECB policy meetings. The distribution of jump sizes is governed by a general multidimensional affine process, enabling analytical tractability and flexibility in capturing interest rate dynamics. However, we choose to adopt a parsimonious model, which is the same as that used in Schlögl et al. (2023), considering a two-dimensional state vector whose components are the expected value of the jump size and its central tendency.

The spread between EURIBOR and €STR is due to the interbank risk that is, the risk

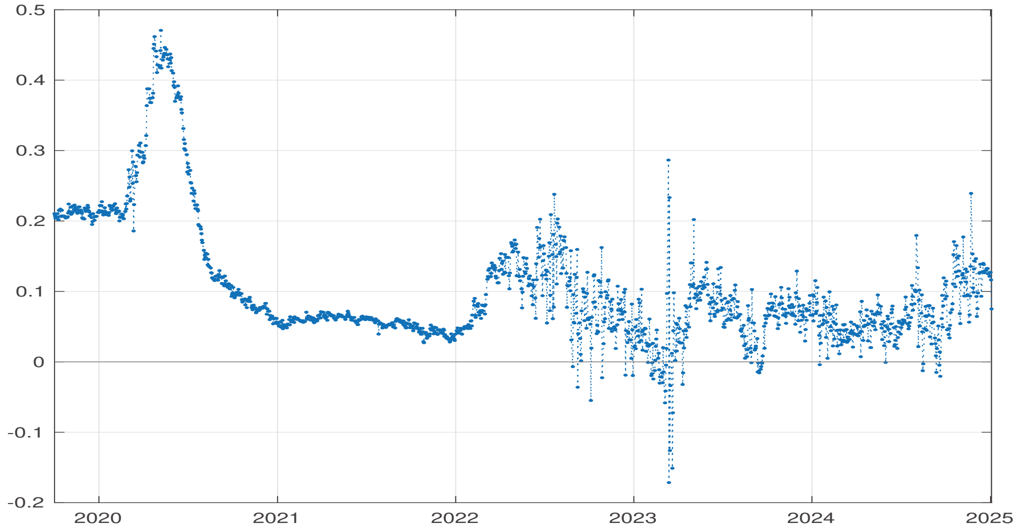

Figure 2: The spread between 3 months EURIBOR and the corresponding OIS on €STR (values are in percentage)

associated to credit and liquidity constraints arising in the exchanges between European banks. We model the term structure of the spread using a one-dimensional affine process. In this way, we are able to jointly fit with a simple model the two term structures. A problem of great practical relevance is related to the measurement of the impact of the possible substitution of EURIBOR with a term rate related to €STR in financial contracts. An aspect of this problem has been studied by Jermann (2024) who addressed the potential impact of the substitution of the LIBOR rate with a term rate linked to SOFR. Kirti (2022) studied the shift from a general IBOR rate to a RFR and developed a model in which the design of reference rates shapes the allocation of risk in equilibrium. With our model, we are able to evaluate, in terms of Value at Risk (VaR), the effect of the substitution of EURIBOR.

We estimate the model on daily term structures on EURIBOR and €STR using the Kalman filter. We assess the performance of the model by measuring the errors in fitting the observed term structures. Its performance is compared against the widely used Dynamic Nelson-Siegel (DNS) model, introduced by Diebold et al. (2006). Despite relying on fewer parameters, the model we propose achieves a superior fit both in-sample and out-of-sample. This confirms the benefit of explicitly accounting for deterministic jumps in modeling short-rate dynamics. The volatility curve of €STR yields from October 2019 to January 2025 has the same snake-shaped form as observed by Piazzesi (2005) on the term structure of US Treasury rates between 1994 and 1998. We also report, as Piazzesi (2005) and Kim and Wright (2014), the existence of a non-homogeneous time effect, related to the increasing of the volatility in the days of the possible jumps, especially for short-term maturities. Our calibrated model reproduces both the observed snake-shaped volatility curve of €STR yields and the non-homogeneous time effects noted on days when jumps may occur. Among the applications of the model, we demonstrate its use in forecasting future rates and estimating the probability distribution of subsequent short-rate changes. We show how the model can be used to assess fallback risk in Forward Rate Agreement (FRA) contracts and we analyze how variations in monetary policy expectations affect yields across different maturities.

In the rest of the paper, Section 2 introduces the model. Section 3 describes the calibration procedure using real data and compares the fitting performance of the proposed model with that obtained by the Dynamic Nelson-Siegel model. Section 4 presents several examples to illustrate some applications of the model. Section 5 concludes. Technical details are in the appendix A.

We complete this section with a review of the contributions that are more relevant to our work.

1.1 Literature review

The interest in this topic is demonstrated by the active involvement of international institutions in the ongoing debate. Among these, the International Capital Market Association (ICMA) has documented the development of RFRs and the transition of legacy LIBOR bonds to these new benchmarks (ICMA, 2023). The International Swaps and Derivatives Association (ISDA) has analyzed the adoption of SOFR, the new reference rate for the US market, and highlighted key industry developments, including synthetic LIBOR rates and term RFRs (ISDA, 2023). The Bank for International Settlements (BIS) has provided a comprehensive primer discussing the robustness and credibility of the new RFRs and their suitability for evolving market needs (BIS, 2019).

From the academic standpoint we cite Klingler and Syrstad (2021) who perform a deep econometric analysis to study the alternative reference rates set to replace LIBOR for different currencies by the end of 2021. Several papers explore how to infer forward-looking term rates from market data related to these new benchmarks. Heitfield and Park (2019) propose a model-free approach to translate SOFR futures prices into indicative forward-looking term rates, similar in concept to the term LIBOR. Skov and Skovmand (2021) also aim to infer forward-looking term rates using dynamic term structure models fitted to SOFR futures data. Studies such as Fontana (2023) analyze derivative pricing under affine models for alternative RFRs, deriving explicit valuation formulas for key financial instruments. Recently, Calvia et al. (2025) developed a PDE-based framework for pricing interest rate derivatives, extending short-rate models to include stochastic discontinuities.

As Backwell and Hayes (2022) write "Interest-rate benchmark reform has revived short-rate modeling. One reason is that short-rate models provide a consistent framework in which different benchmarks, and contracts linked to them, can be compared. Another reason is that new benchmarks can be directly dependent on very short-term rates". Short rate affine models provide a flexible and tractable framework for modeling the yield curve under no-arbitrage. Piazzesi (2010) offers a comprehensive review of the methodology. These models have been widely used to characterize the dynamics of interest rates and their interaction with macroeconomic fundamentals. However, the standard affine diffusion framework struggles to replicate the observed behavior of yields at short maturities, particularly around scheduled monetary policy events. Looking at the SOFR futures and options market, Gellert and Schlögl (2021) and Brace et al. (2024) construct models where the short rate is constant between known jump times, such as scheduled Federal Open Market Committee (FOMC) meetings, while forward rates evolve diffusively, reconciling these seemingly contradictory observations. Piazzesi (2001) and Piazzesi (2005) propose a model with jumps occurring during the period of the FOMC meeting to study the interconnection between bond yields and monetary policy. The Fed's target rate is modeled as a jump process with discrete values with intensities that depend on the state of the economy and the meeting calendar of the FOMC. The model explains the “snake” shape of the volatility curve, the standard deviation of yield changes as a function of maturity, observed in the data, with inertia in monetary policy. She also documents a calendar effect in the volatility curve around FOMC meetings. The volatility curve shifts up around these meetings, especially at short maturities. The model matches this seasonality with monetary policy shocks, which happen mostly at these meetings. Kim and Wright (2014) also report a hump in the volatility curve for the U.S treasury yields on U.S. employment report days, as well as an increase on the same dates. To explain these empirical facts, they propose a model that allows all elements of the state vector to jump at known times, and allows the pricing kernel to jump as well.

Analogously to the work of Piazzesi, Backwell and Hayes (2022) model the short rate as a jump process with discrete values. The jump probability distribution depends on a diffusive state variable that represents market views. Their work focuses on SONIA, the new RFR for the Sterling market, and on the pricing of caplets which show a time-inhomogeneous behavior due to the expected jumps of the short rate. Schlögl et al. (2023) use a model that can be nested in the general framework of Kim and Wright (2014) to study the U.S. SOFR market. They show that including jumps at FOMC meetings leads to significant gains in fitting the term structure. Moreover, Fontana et al. (2020) and Fontana et al. (2024) develop a general multicurve term structure framework with stochastic discontinuities, including both deterministic and inaccessible jumps, using an extended HJM approach, providing valuation formulas and exploring hedging strategies.

To study the decomposition of the interbank risk into its two main components, that is, credit and liquidity, Filipović and Trolle (2013) develop a multicurve affine model for the term structure of interbank risk, drawing on IRS, OIS and CDS data. They find that while the non-default component is important at the short end during crisis periods, default risk is a dominant driver at longer maturities. With a similar approach, Skov and Skovmand (2023) jointly models SOFR, EFFR, LIBOR and term repos, and find that the spread during the pandemic was mainly due to credit risk, while on average credit and funding-liquidity risk contribute equally to the spread.

2 The model

To model the €STR term structure we assume the existence of a short rate process r_t defined on a filtered probability space $\left(\Omega, \mathcal{F}, \{\mathcal{F}\}_{t\geq 0}, P\right)$. We observe from Figure 1 that the time series of €STR is roughly constant, with changes occurring only at pre-scheduled times, six days after the central bank monetary policy meetings. Hence, we set

$$dr_t = J_t dN_t$$

where N_t is a counting process with jumps at deterministic times, that is, $dN_t = 1$ if $t \in \mathcal{T}$ and $dN_t = 0$ otherwise, where the set $\mathcal{T}$ contains all the times where a change in the short-term rate may occur. For $t \in \mathcal{T}$, the jump size is

$$J_t = a' X_t + w\epsilon_t, \tag{1}$$

where w is a scalar, a is a D-dimensional vector, a' its transpose, and ϵ_t are i.i.d. standard normal, independent of the process X. The state process X_t, that drives the dynamics of r_t, is a D-dimensional affine process with conditional moment generating function

$$\mathbb{E}_t \left[\exp\left(u' X_T\right)\right] = \exp\left(\Phi(T-t,u) + \Psi(T-t,u)' X_t\right),$$

and $\Phi(\cdot,\cdot)$, $\Psi(\cdot,\cdot)$ are deterministic functions.

Since r_t represents the short-term interest rate, the €STR zero-coupon yield at time t with maturity T is

$$y^{€STR}(t,T) \quad = \quad -\frac{\log(\mathbb{E}_t^Q \left[\exp(-\int_t^T r_u du)\right])}{T-t}$$

where $\mathbb{E}_t^Q$ represents the expectation with respect to the risk neutral probabilities Q. We assume that the change of measure from P to Q is such that the process X maintains the affine property under the risk-neutral measure Q, that is,

$$\mathbb{E}_t^Q[\exp\left(u' X_T\right)] = \exp\left(\Phi^Q(T-t,u) + \Psi^Q(T-t,u)' X_t\right). \tag{2}$$

where $\Phi^Q(\cdot,\cdot)$, $\Psi^Q(\cdot,\cdot)$ are deterministic functions.

The short rate process that models the EURIBOR term structure is obtained by adding the process s_t to r_t. The spread s_t is modeled by a process that is affine and independent of X_t, under both the probability measures. The EURIBOR zero-coupon yield at time t with maturity T is

$$\begin{aligned} y^{EURIBOR}(t,T) \quad &= \quad -\frac{\log(\mathbb{E}_t^Q \left[\exp(-\int_t^T (r_u + s_u) du)\right])}{T-t} = \\ &= \quad y^{€STR}(t,T) - \frac{\log(\mathbb{E}_t^Q \left[\exp(-\int_t^T s_u du)\right])}{T-t}. \end{aligned}$$

Under the assumptions of the model, it is possible to efficiently compute the yield of a zero-coupon bond for both structures, €STR and EURIBOR. The following result provides the backward algorithm for the €STR yields. It is a particular case of Proposition 1 in Kim and Wright (2014) and we report it adapted to our framework for the convenience of the reader. The proof follows from the affine property of the state value process X and it is shown in Appendix A.1.

Proposition 1. *Let $T_1 < T_2 \cdots < T_n$ be the possible jump times in the interval $[t, T)$, then*

$$y^{€STR}(t,T) = r_t - \frac{1}{T-t}\left(G(T_1,\ldots,T_n,T) + \Phi^Q(T_1 - t, F(T_1,\ldots,T_n,T))\right)$$
$$- \frac{1}{T-t}\Psi^Q(T_1 - t, F(T_1,\ldots,T_n,T))' X_t \tag{3}$$

where the functions $G(T_1,\ldots,T_n,T)$ and $F(T_1,\ldots,T_n,T)$ are obtained by backward recursion, starting from

$$G(T_n,T) = \frac{1}{2}w^2(T-T_n)^2$$
$$F(T_n,T) = -(T-T_n)a,$$

and continuing with

$$G(T_k,\ldots,T_n,T) = \frac{1}{2}w^2(T-T_k)^2 + G(T_{k+1},\ldots,T_n,T) +$$
$$+ \Phi^Q(T_{k+1} - T_k, F(T_{k+1},\ldots,T_n,T))$$
$$F(T_k,\ldots,T_n,T) = -(T-T_k)a + \Psi^Q(T_{k+1} - T_k, F(T_{k+1},\ldots,T_n,T))$$

Of course, the times of possible jumps $T_i \in \mathcal{T}$ $i = 1,\ldots,n$ depend on t and T but to simplify the notation we do not explicate such dependence. We remark that $y^{€STR}(t,T)$ is equal to r_t when there are no jump dates between t and T.

The yield on EURIBOR is

$$y^{EURIBOR}(t,T) = y^{€STR}(t,T) - \frac{A(t,T) + B(t,T)s_t}{T-t} \tag{4}$$

where $A(\cdot,\cdot)$ and $B(\cdot,\cdot)$ are deterministic functions that depend on the specific affine process chosen for s_t.

To derive a formula for the unconditional variance of the €STR term structure we write Equation (3) as (dropping the subscript €STR)

$$y(t,T) = d^X(t,T) + r_t + Z^X(t,T)X_t, \tag{5}$$

where

$$d^X(t,T) = -\frac{1}{T-t}\left(G(T_1,\ldots,T_n,T) + \Phi^Q(T_1 - t, F(T_1,\ldots,T_n,T))\right)$$
$$Z^X(t,T) = -\frac{1}{T-t}\Psi^Q(T_1 - t, F(T_1,\ldots,T_n,T))'.$$

Let Δ_h denote the time difference operator with step size $h > 0$. For a function $u(t,T)$ depending on two time variables t and T, we define:

$$\Delta_h u(t,T) := u(t+h, T+h) - u(t,T).$$

That is, the operator advances both arguments by h before computing the difference. We also write Δ_h for the standard difference operator when applied to functions of a single variable $v(t)$. In this case, obviously:

$$\Delta_h v(t) := v(t+h) - v(t).$$

Let us define

$$C := \Delta_h Z^X(t,T), \qquad D := Z^X(t+h,T+h).$$

Both C and D, as well as $\Delta_h d^X(t,T)$, depend on t, T and h, but we omit this dependence for ease of notation. Assuming that the next possible jump takes place at a time T_J, we can express the change in yield in Equation (5) as

$$\Delta_h y(t,T) = \Delta_h d^X + C' X_t + D' \Delta_h X_t + J_{T_J} \delta_{t<T_J<t+h}, \tag{6}$$

where $\delta_{t<T_J<t+h}$ is the indicator function that accounts for a jump that occurs in the time interval $(t, t+h)$.

Dropping the dependence on t, T to simplify the notation, the unconditional variance of $\Delta_h y$ is

$$\begin{aligned} \mathrm{Var}[\Delta_h y] &= \mathrm{Var}[C' X_t + D' \Delta_h X_t + J_{T_J} \delta_{t<T_J<t+h}] \\ &= \mathrm{Var}[C' X_t + D' \Delta_h X_t] + \left(\mathrm{Var}[J_{T_J}] + 2\mathrm{Cov}[C' X_t + D' \Delta_h X_t, J_{T_J}]\right) \delta_{t<T_J<t+h}. \end{aligned} \tag{7}$$

Equation (7) separates the diffusive component of the variance, that is always present, from that of the jump, appearing only when the next possible jump is in the time interval $(t, t+h)$. The diffusive component of the variance is

$$\mathrm{Var}[C' X_t + D' \Delta_h X_t] = C' \mathrm{Var}[X_t] C + 2C' \mathrm{Cov}[X_t, \Delta_h X_t] D + D' \mathrm{Var}[\Delta_h X_t] D.$$

As for the components related to the jump,

$$\begin{aligned} \mathrm{Var}[J_{T_J}] &= \mathrm{Var}[a' X_{T_J}] + \mathrm{Var}[\omega \varepsilon] \\ &= a' \mathrm{Var}[X_{T_J}] a + \omega^2. \end{aligned}$$

Moreover,

$$\begin{aligned} \mathrm{Cov}[C' X_t + D' \Delta_h X_t, J_{T_J}] &= \mathrm{Cov}[C' X_t + D' \Delta_h X_t, a' X_{T_J}] \\ &= C' \mathrm{Cov}[X_t, X_{T_J}] a + D' \mathrm{Cov}[\Delta_h X_t, X_{T_J}] a. \end{aligned}$$

Substituting into Equation (7), we get the explicit formula for the unconditional variance

$$\begin{aligned} \mathrm{Var}[\Delta_h y] = {} & C' \mathrm{Var}[X_t] C + 2C' \mathrm{Cov}[X_t, \Delta_h X_t] D + D' \mathrm{Var}[\Delta_h X_t] D + \\ & + \left(a' \mathrm{Var}[X_{T_J}] a + \omega^2 + C' \mathrm{Cov}[X_t, X_{T_J}] a + D' \mathrm{Cov}[\Delta_h X_t, X_{T_J}] a\right) \delta_{t<T_J<t+h}. \end{aligned} \tag{8}$$

The components of this expression, explicitly computed for the specific model to be presented in Section 3.2, are provided in Appendix A.3.

3 Model calibration

In this section we specify a particular instance of the general modeling framework and calibrate it to the data. We begin by presenting the dataset, followed by a detailed description of the model and the calibration procedure. Next, we evaluate the model's performance against a benchmark, considering both in-sample and out-of-sample results. The section concludes with an analysis of the yield volatility curves, comparing the observed patterns to those implied by the model.

3.1 The data

We consider the daily time series of the term structures of €STR and of EURIBOR from October 2, 2019, which is the first day €STR was published, to January 6, 2025. For each day in the sample and for both term structures, we consider the zero-coupon yields with maturities 1 day, 2 days, 1 week, 1 month, 3 months, 6 months, 9 months, and from 1 to 10 years. These are, for each day, 17 yields with different maturities for each term structure, a total of 34 yields. The two term structures have been constructed by Datastream from, respectively, the OIS rates indexed on €STR and from the deposit rates and the IRS rates indexed on the 6 month EURIBOR.

Figure 3 displays the time series of the €STR term structure (Panel A) and of the EURIBOR term structure (Panel B). We divide the time period into "Period I", going from the beginning of the sample to September 14, 2022 and "Period II", containing the remaining part of the series. As we can see from Figure 1, Period I is characterized by short-term rates that are almost constant at level zero or negative, while in Period II they are increasing, then constant for a while and decreasing towards the end of the period.

3.2 Model specification

We adopt a model with four factors, denoted by $r_t, \xi_t, \theta_t, s_t$, which we call the "4F-model", which is an instance of the general framework presented in Section 2. It is obtained by defining the vector X_t in Equation (1) as a 2-dimensional process $X_t = (\xi_t, \theta_t)'$, and by setting $a' = (\gamma, 0)$, where γ is a scale parameter that multiplies the jump size under the objective measure. As in Schlögl et al. (2023), we fix this parameter to one in the risk neutral measure. The process ξ_t represents, for $t \in \mathcal{T}$, the expected value under Q of the normally distributed jump J_t, and θ_t is its central tendency factor. Under the risk-neutral measure Q the dynamics of the state variables are

$$d\xi_t = \kappa^\xi(\theta_t - \xi_t)dt + \sigma^\xi dW_t^\xi \tag{9}$$

$$d\theta_t = \kappa^\theta(\bar{\theta} - \theta_t)dt + \sigma^\theta \left(\rho dW_t^\xi + \sqrt{1-\rho^2}dW_t^\theta\right) \tag{10}$$

Moreover, we set the dynamics of the spread as

$$ds_t = \kappa^s(\bar{s} - s_t)dt + \sigma^s dW_t^s \tag{11}$$

where $W_t^Q = (W_t^\xi, W_t^\theta, W_t^s)$ is a three-dimensional vector of independent standard Brownian motions under the risk-neutral measure Q. We impose a change of measure that preserves the

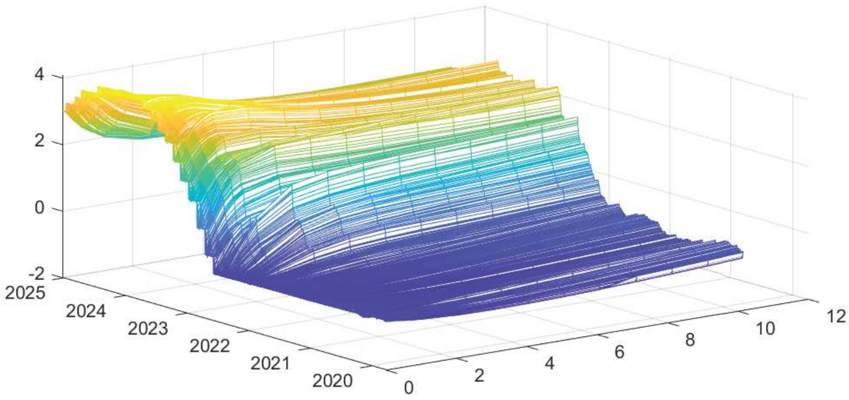

(a) Panel A: € STR

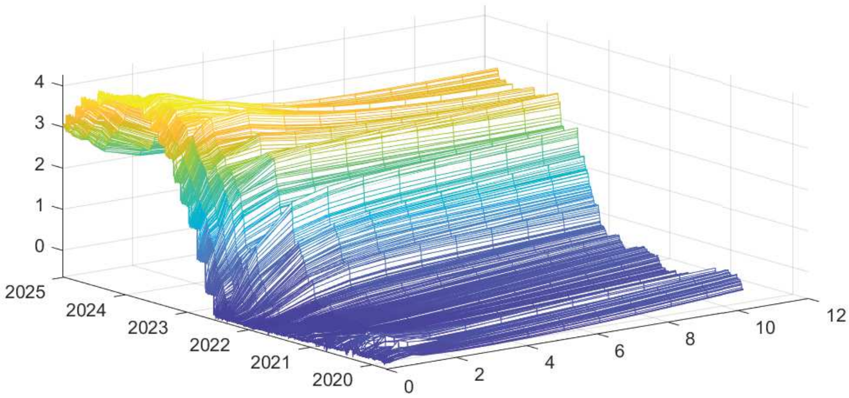

(b) Panel B: Euribor

Figure 3: Time series of the € STR (Panel A) and Euribor (Panel B) term structures on which the model is estimated. Rates on the vertical axis are expressed in percentage terms, maturities are expressed in years.

affine structure by introducing a constant market prices of risk $\Lambda = (\lambda^{\xi}, \lambda^{\theta}, \lambda^{s})$ such that the process

$$W_t^P = W_t^Q - \Lambda t \tag{12}$$

is a standard Brownian motion under the objective measure P.

Except for the spread, the 4F-model belongs to the general framework introduced by Kim and Wright (2014) and it was also used by Schlögl et al. (2023) to analyze the term structure of SOFR. From a computational point of view, the main advantage of this model specification is that the characteristic function of $X_t = (\xi_t, \theta_t)'$

$$\mathbb{E}_t^Q\left[e^{u'X_T}\right] = \exp\Big(\Phi^Q(\tau, u) + \Psi^Q(\tau, u)'X_t\Big), \qquad \tau := T - t,\ u = (u_1, u_2)', \tag{13}$$

can be obtained in closed form. In fact, let us express the dynamics of X_t in matrix form

$$dX_t = K(\bar{X} - X_t)\,dt + \Sigma_X\,dW_t, \tag{14}$$

with

$$K = \begin{bmatrix} \kappa^{\xi} & -\kappa^{\xi} \\ 0 & \kappa^{\theta} \end{bmatrix},\ \Sigma_X = \begin{bmatrix} \sigma^{\xi} & 0 \\ \rho\sigma^{\theta} & \sqrt{1-\rho^2}\sigma^{\theta} \end{bmatrix},\ \bar{X} = \begin{bmatrix} \bar{\theta} \\ \bar{\theta} \end{bmatrix}.$$

Hence, the coefficients of the characteristic function (13) satisfy the system of Riccati equations

$$\begin{aligned}
\partial_\tau \Psi^Q(\tau, u) &= -K'\Psi^Q(\tau, u), \\
\partial_\tau \Phi^Q(\tau, u) &= \tfrac{1}{2}\,\Psi^Q(\tau, u)'\Sigma_X\Sigma_X'\,\Psi^Q(\tau, u) + \kappa^{\theta}\bar{\theta}\,\Psi_2^Q(\tau, u).
\end{aligned}$$

Therefore,

$$\begin{aligned}
\Psi_1^Q(\tau, u) &= u_1\,e^{-\kappa^{\xi}\tau} \\
\Psi_2^Q(\tau, u) &= u_2\,e^{-\kappa^{\theta}\tau} + \frac{\kappa^{\xi}}{\kappa^{\theta} - \kappa^{\xi}}\,u_1\big(e^{-\kappa^{\xi}\tau} - e^{-\kappa^{\theta}\tau}\big),
\end{aligned}$$

and the term Φ^Q is obtained by

$$\Phi^Q(\tau, u) = \int_0^{\tau}\Big(\tfrac{1}{2}\,\Psi^Q(s, u)'\Sigma_X\Sigma_X'\,\Psi^Q(s, u) + \kappa^{\theta}\bar{\theta}\,\Psi_2^Q(s, u)\Big)\,ds,$$

where we assume that $\kappa^{\theta} \neq \kappa^{\xi}$ and, in the case $\kappa^{\theta} = \kappa^{\xi}$, we can take the continuous limit as $\kappa^{\theta} - \kappa^{\xi} \to 0$.

Since Ψ^Q is a linear combination of exponentials, the integral is elementary and, for brevity, we do not provide its explicit representation here.

3.3 Calibration results

We calibrate the 4F-model using the Kalman filter, as described in Appendix A.2, considering both the entire sample period and the two sub-periods defined in Section 3.1. Table 1 reports the resulting parameter estimates, where a double asterisk indicates statistical significance at the 5% level.

Parameter	Whole sample	Period I	Period II
κ^ξ	1.5042**	1.6069**	1.1968**
σ^ξ	0.0043731**	0.0039879**	0.0053183**
κ^θ	1.3578**	1.4475**	1.292**
$\bar{\theta}$	0.00020136**	0.00018001**	0.00042571**
σ^θ	0.0033399**	0.0032268**	0.0031833**
κ^s	1.5686**	1.4587	1.6193**
$\bar{s}$	0.0023041	0.0024495	0.0021631
σ^s	0.028976**	0.028269**	0.030509**
w	0.0020732**	0.002005**	0.0020783**
ρ	-0.89996**	-0.89996**	-0.89996**
σ	0.00051719**	0.00043421**	0.00051443**
λ^ξ	0.00023246	0.00038377	0.00018659
λ^θ	-0.00016896	1.0416e-05	-0.00022283
λ^s	-3.7504e-05	-5.8424e-05	-1.2512e-05
γ	0.99929**	0.99931**	0.99982**

Table 1: Parameter Estimates. Statistical significance at the 5% level is denoted by **.

The estimates of the risk-neutral parameters are, in general, statistically significant for the whole sample and for the two sub-periods. The exceptions are the estimates of parameter $\bar{s}$ for all the samples, and that of κ^s on Period I. The estimates for the market price of risk parameters $\lambda^\xi, \lambda^\theta, \lambda^s$ are not significant, suggesting that the data do not provide sufficient evidence to distinguish between the objective and the risk-neutral measure. Similar difficulties in identifying the parameters of the market prices of risk have also been reported by Filipović and Trolle (2013). Also, the parameter γ that multiplies the jump size in the objective measure is not significantly different from 1, which is the value set under the risk-neutral measure.

The diffusion parameters of the dynamics of ξ and θ are small, of the order of 10^{-3}, while that of the spread is of the order 10^{-2}, implying a non-negligible volatility for the dynamics of the EURIBOR term structure. The estimated speed of mean reversion in ξ is $\kappa^\xi = 1.5042$ (on the whole sample), which amounts to a daily autoregressive coefficient $\exp(-\kappa^\xi/250) = 0.994$ and a half-life of shocks to ξ approximately equal to half a year, that is, $\frac{\ln(2)}{\kappa^\xi} = 0.46$ years. Similarly for the corresponding estimates on Period I and Period II, with autoregressive coefficients respectively of 0.994 and 0.995 and a half-life of shocks respectively of 0.43 and 0.58 years. In period II the half-life time reaches its peak and, therefore, in that period the process ξ reverts more slowly to its mean. When the rates are flat, in Period I, the process ξ reverts faster. A similar pattern can be seen for the process θ (its half-life on the whole sample is 0.51 years, in Period I is 0.48 years and in Period II is 0.54 years). With regard to the spread process s, the speed of mean reversion is higher in Period II than in the other samples: for the whole sample the half-life is 0.44 years, for Period I is 0.48 years and for Period II is 0.43 years. The correlation between processes ξ and θ is strongly negative in all samples, and this fact is apparent in Figure 5 where the paths of the estimated state variables are shown.

We measure the capability of a model (the 4F-model and that used as a comparison in the sequel) to fit the data by computing the squares of the errors for each day and each maturity in the sample, that is, we take the squares of the residuals in the model's measurement equation (for the 4F-model, Equation 22). We compute two metrics: (i) the mean squared error across maturities for each day, and (ii) the sample mean of squared errors for each maturity, a standard measure also used by Schlögl et al. (2023). We also take the square root of both metrics to obtain the root mean squared errors (RMSE).

Figure 4 reports two examples of the fitting capability of the model. We select two days (July 26, 2023 and September 4, 2024) when the curves have different shapes and such that the cross-sectional RMSE is 4.5 basis points, which is close to its sample mean. Data about €STR are on the left panels, while those about EURIBOR are on the right ones. We see that the model is able to reproduce both types of structures.

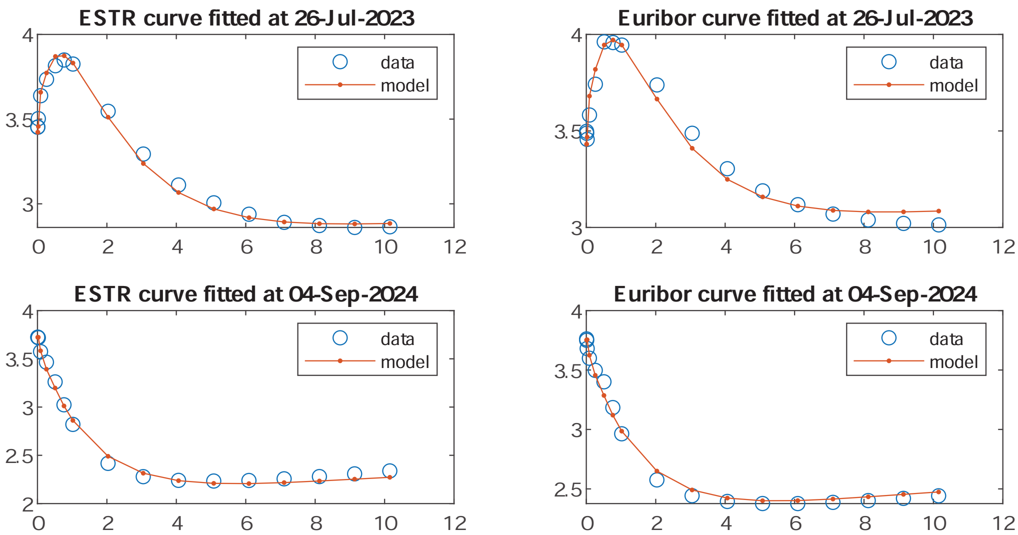

Figure 4: The 4F-model fitted to the data for two particular days, July 26, 2023 and September 4, 2024. The €STR curves are on the left panels, the EURIBOR curves on the right panels. The maturities on the x-axis are expressed in years. Rates on the y-axis are in percentage terms.

Table 2 shows the RMSE of yields for a set of representative maturities, across the two term structures and the three sample periods considered.

Figure 5 reports the time series of the four estimated latent variables of the model calibrated on the entire sample. We see that the variable r_t (top right), representing the short rate, is in fact closely related to the €STR, or to the Deposit Facility rate (Figure 1). The variable ξ_t (top left) drives the expected values of changes in the variable r_t. We see that after a first period where its path is almost flat and close to zero, it increases steadily at the beginning of 2022, reaches a peak during the second half of 2022, and then reverts to negative values in the second half of 2024,

Maturity	1D	1W	1M	6M	1Y	2Y	5Y	7Y	10Y
Panel A: Whole sample									
€STR	3.7	3.6	3.8	4.7	4.6	6.8	3.2	3.3	5.6
EURIBOR	5.2	3.8	6.2	9.2	4.2	6.8	3.7	2.5	5.0
Panel B: Period I									
€STR	3.7	3.6	3.8	4.8	4.3	6.5	3.1	3.5	5.9
EURIBOR	4.5	3.0	4.0	8.2	4.0	6.9	4.3	2.7	4.5
Panel C: Period II									
€STR	3.6	3.7	3.6	5.4	5.5	7.0	3.1	2.0	4.9
EURIBOR	5.4	4.7	8.1	10.3	4.3	5.6	2.9	2.4	4.5

Table 2: Root mean squared errors (in basis points) for different maturities, computed over the three sample periods: the full sample (Panel A), Period I (Panel B), and Period II (Panel C).

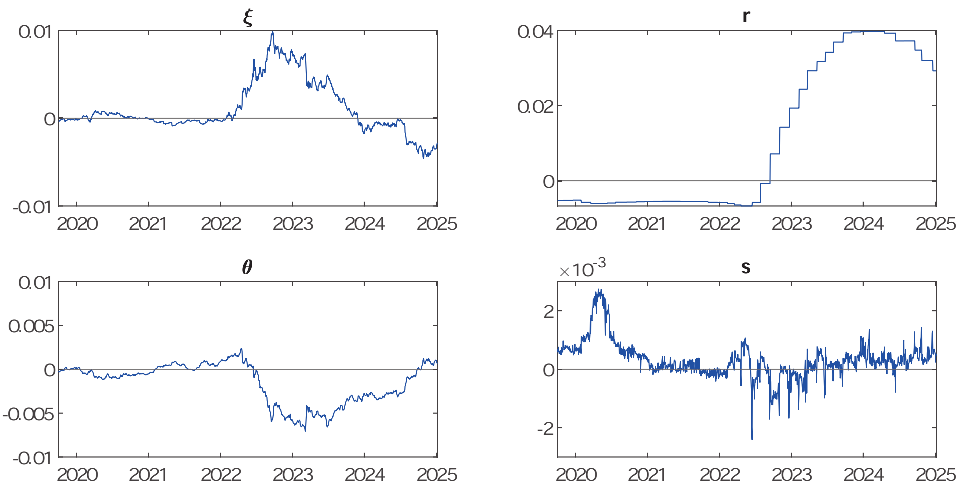

Figure 5: The paths of the estimates of the four state variables, ξ_t (top left), θ_t (bottom left), r_t (top right), s_t (bottom right).

when it was expected that the ECB was about to lower official rates. The variable θ_t (bottom left) represents the long-term mean of the variable ξ_t. It is apparent that the two variables are strongly negatively correlated, reflecting the fact that, if a movement is expected on the policy rate, that movement will be slowly reverted in the future. The spread s_t (bottom right) is positively correlated, as expected, with the observed spread between the 3 months EURIBOR and the 3 months euroSTR-based OIS (Figure 2). The correlation coefficient between the latent factor s_t and the spread between the zero-coupon yields with maturity 3 months is 0.81.

3.4 The benchmark: Dynamic Nelson Siegel model

We adopt a widely used model for yield curve fitting as a benchmark, the Nelson-Siegel model (Nelson and Siegel (1987)), specifically its dynamic version introduced by Diebold et al. (2006), to which we refer for further details.

The Nelson-Siegel expression of the yield to maturity is

$$y(t,T) = \beta_1 + \beta_2 \left(\frac{1 - e^{-\lambda(T-t)}}{\lambda(T-t)} \right) + \beta_3 \left(\frac{1 - e^{-\lambda(T-t)}}{\lambda(T-t)} - e^{-\lambda(T-t)} \right)$$

where λ is a parameter to be estimated. The three latent factors $f = (\beta_1, \beta_2, \beta_3)'$ can be interpreted respectively as level, slope and curvature factors. In the dynamic version of the Nelson-Siegel model, henceforth DNS, such factors are assumed to follow a vector autoregressive process of first order

$$f_{i+1} - \mu = \Gamma(f_i - \mu) + \eta_i, \qquad i = 1, \dots, N_{obs}$$

where Γ and μ are matrices of conformable dimensions, η is a normal shock, and i labels observation times.

Since the 4F-model aims to jointly reproduce the term structures of both €STR and EURIBOR, we fit the DNS model separately to each curve. Specifically, we use a 3-factor DNS model to fit the €STR curve and a different 3-factor DNS model to fit the EURIBOR curve. The DNS model is estimated via Kalman filter.

We adopt a particular specification of the DNS model in which all matrices are assumed to be diagonal, and the standard deviation of the measurement error is assumed to be constant across maturities, mirroring the assumptions made in the 4F-model. In total, the benchmark model includes 22 parameters: 11 for calibrating the €STR curve and 11 for the EURIBOR curve. In contrast, the 4F-model we aim to test against the benchmark uses only 15 parameters. These include nine parameters that govern the dynamics of ξ, θ and s, the standard deviation of the jump component w, the standard deviation of the measurement error σ, the coefficient γ, and the market prices of risk associated with ξ, θ and s. Even though the 4F-model has fewer parameters to describe the observations, it incorporates information about the known jump dates, which may give it an advantage over the benchmark.

3.5 In- and out-of sample fitting performance

Figure 6 shows the performance of the 4F-model compared to the DNS benchmark. The analysis considers both in-sample and out-of-sample performance when fitting the €STR yield curve (left

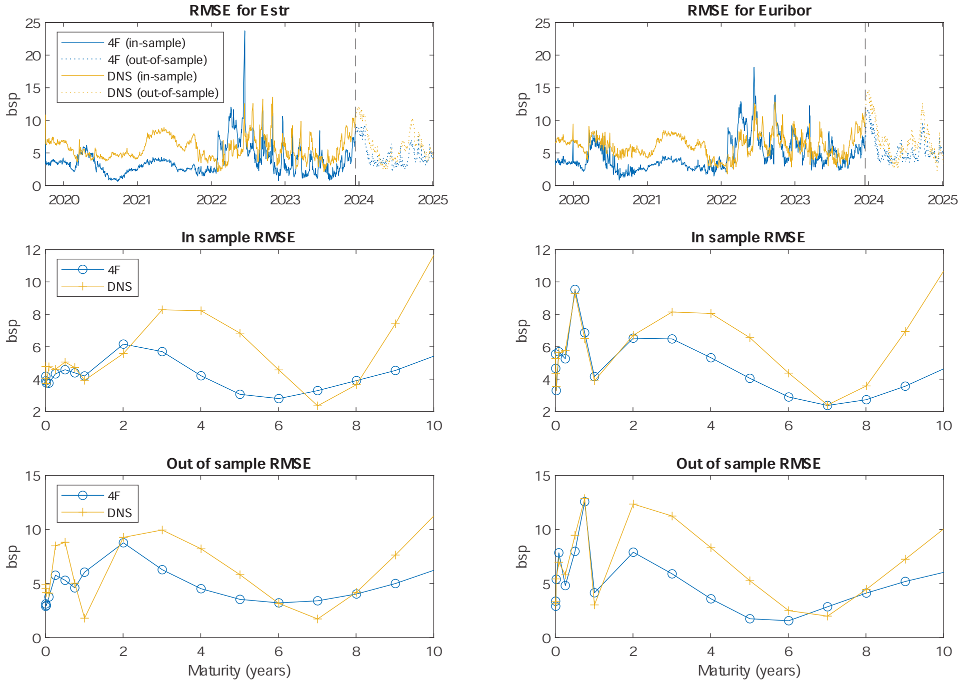

Figure 6: In- and out-of-sample fit performance for the benchmark model (DNS) and the 4F-model model. The upper panels show the cross-sectional root mean squared error at each time point, obtained by fitting the models to the €STR term structure (left) and EURIBOR (right). Calibration is performed using 80% of the observations. The term structure is then reconstructed via the Kalman filter both in-sample and out-of-sample. The middle panels display the in-sample root average (across time) squared errors for each maturity, while the bottom panels refers to the out-of-sample performance. All errors are expressed in basis points.

panels) and the EURIBOR (right panels). The calibrations of both models are carried out using the first 80% of the observations via the Kalman filter. Afterwards, we construct the yield curves from the estimated models both in-sample (i.e., within the estimation window) and out-of-sample (i.e., on the holdout set). The upper panels of Figure 6 display the cross-sectional root mean squared error for each sample date. In addition, we assess the average performance over time by examining the square root of mean squared errors for each maturity. The results are shown in Figure 6 with in-sample results displayed in the middle panels and out-of-sample results in the bottom panels. All errors are reported in basis points to facilitate interpretation. The results show clearly that, with some exceptions, the 4F-model outperforms the benchmark model both in-sample and out-of-sample.

For a comparison of the fitting performances of the two models, we also perform a t-test on the difference in squared fitting errors, specifically, the difference between the squared error of the 4F-model from that of the benchmark. The results are reported in Table 3. In the in-sample analysis, the test indicates that the 4F-model fits the €STR yield curve better than the benchmark in eleven out of fifteen significant cases, as evidenced by predominantly negative test statistics. For the EURIBOR curve, the 4F-model outperforms the benchmark in ten out of fourteen significant cases. Out-of-sample, the 4F-model performs even better. For the €STR curve, the benchmark is preferred only for the 1-year and 7-year maturities; for all other maturities, the 4F-model shows superior performance. In the case of the EURIBOR curve, the benchmark outperforms the 4F-model also at the 1-month maturity. The last row of Table 3 reports the results of the test aggregated across both time and maturities. The test favors the 4F-model both in-sample and out-of-sample.

	€ STR		EURIBOR	
Maturity	In-Sample	Out-of-Sample	In-Sample	Out-of-Sample
1 day	-3.08***	-9.21***	1.67*	0.39
2 days	0.55	-5.69***	2.24**	-1.83*
1 week	0.10	-4.91***	-2.18**	-0.25
1 month	-3.01***	-1.52	0.29	3.68***
3 months	-1.12	-11.44***	-3.43***	-6.12***
6 months	-3.71***	-12.62***	1.42	-15.72***
9 months	-3.31***	-1.49	2.74***	-2.89***
1 year	2.86***	21.14***	2.10**	7.402***
2 years	4.59***	-4.11***	-0.97	-15.41***
3 years	-15.52***	-15.79***	-8.43***	-14.86***
4 years	-27.54***	-13.39***	-16.49***	-14.83***
5 years	-35.83***	-10.94***	-22.34***	-16.35***
6 years	-25.24***	0.37	-19.82***	-8.70***
7 years	11.05***	16.97***	-0.38	8.40***
8 years	2.015**	-1.91*	-11.45***	-1.57
9 years	-19.50***	-19.44***	-27.23***	-6.60***
10 years	-35.85***	-26.61***	-35.17***	-10.21***
all maturities	-8.43***	-6.85***	-6.69***	-5.90***

Table 3: t-test comparing the fit performance of the 4F-model against the benchmark DNS model. The table reports the test statistics both in-sample and out-of-sample across different maturities. Negative values of the statistic indicate that the 4F-model outperforms the benchmark. Statistical significance at the 10%, 5%, and 1% levels is denoted by *, **, and ***, respectively.

3.6 Volatility of yields

Figure 7, left panel, represents the sample volatility curves of the €STR term structure. Considering the whole sample, we compute the standard deviation of the daily changes of the €STR term structure by separating the periods that include dates of possible jump from the others. We observe two main features. The first is that the volatility curve estimated only for the possible jump dates is higher than that computed by considering all other dates. The second is that that

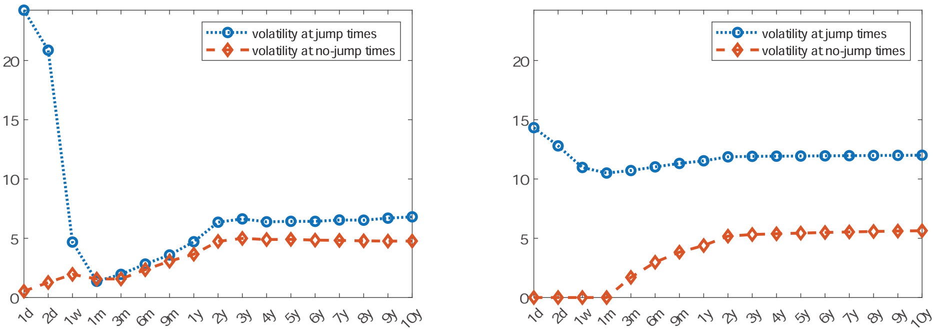

Figure 7: Volatility curves. Standard deviation of daily changes of the €STR term structure calculated on possible jump dates (dotted lines) and on the remaining ones (dashed lines) as a function of the maturity. The left panel shows the sample volatility curves. The right panel displays the unconditional values implied by the model as given in Equation (8). The values on the y axis are in basis points.

it presents the characteristic "snake shape", as it was defined by Piazzesi (2005), that is very high at the short end, rapidly decreasing and then increasing, with a hump for maturities around 3 years, and with a flat tail for longer maturities. The different volatility regimes in periods that include possible jumps have been observed also by Kim and Wright (2014), on daily data in the period 1990-2007, on the term structure of US Treasury yields from 3 months to 10 years, with possible jumps on employment report dates, and by Piazzesi (2005) on weekly data from the US-LIBOR term structures extracted from swap rates with maturities from 1 month to 5 years, from 1994 to 1998.

Both the change in the volatility regime and the "snake shape" of the volatility curve can be regarded as stylized facts of volatility curves of term structures connected with processes with possible jumps at deterministic times. Hence, these features should be considered essential characteristics in interest rate term structure models.

To demonstrate that the 4F-model is able to reproduce both the features, we compute the volatility of yield variations given by the model, by taking the square root of the unconditional variance provided in formula (8). When the state process X is specified as in (14), and with $a' = (\gamma, 0)$, all terms contributing to the variance in (8) can be computed explicitly. The full derivations are provided in Appendix A.3.

The model-implied volatility, computed using parameters calibrated to the data, is shown in the right panel of Figure 7. We observe that the volatility curves are snake-shaped on jump dates and hump-shaped on non-jump dates, consistent with the empirical patterns seen in the left panel. Furthermore, volatility levels are noticeably higher on jump dates compared to non-jump dates. The long-term volatility in the jump case is about 5 basis points higher than the corresponding empirical estimates. This discrepancy may be caused by the fact that the empirical estimates are based on a sample period that includes extended sub-periods of flat interest rates.

4 Applications

In this section we show some applications of the 4F-model. First, we evaluate the forecast performance of the 4F-model in comparison with that of the dynamic Nelson Siegel model (Section 4.1). We also evaluate the probability distribution of possible future jump sizes (Section 4.2). Then, we address the problem of computing the so-called fallback risk (Section 4.3). Finally, we study how variations in the expected jump affect the entire term structure (Section 4.4).

4.1 Performance in term structure forecasting

We evaluate the performance of the 4F-model in forecasting the entire term structure and compare it to the benchmark model of Section 3.4. Table 4 presents the results of this comparison for both €STR (Panel A) and Euribor (Panel B). The table reports the root mean square errors (in basis points) for both models across different forecast horizons (in days), as well as the Diebold-Mariano statistics (Diebold and Mariano (1995)) with significance levels indicated at 10% (*), 5% (**), and 1% (***). The test is based on the difference between the squared forecast errors of the 4F-model and those of the benchmark. Therefore, a negative and statistically significant value of the test statistic indicates that the 4F-model outperforms the benchmark. The models are estimated using 80% of the available data, while the forecast accuracy is evaluated out-of-sample, either across all time points (left panel) or only at those time points for which at least one ECB meeting date occurs between the forecast origin and the horizon (right panel).

When all time points are used to perform the test, we observe that the benchmark model outperforms the 4F-model in forecasting the yield curves (either €STR or Euribor) over shorter horizons (10 or 20 days). However, for longer horizons (30 and 60 days), the 4F-model provides better forecasts. A possible explanation is that, over shorter horizons, the ECB meetings are not so frequent. In this setting, the benchmark model – which includes six factors compared to only four in the 4F-model – has an advantage. In contrast, on longer horizons, the likelihood of a meeting occurring between the evaluation time and the forecast horizon increases and the 4F-model is better equipped to handle such scenarios.

To emphasize this point, we repeat the Diebold-Mariano test by restricting the evaluation to those instances where a meeting occurs within the forecast horizon. In this reduced sample, the 4F-model is expected to outperform the benchmark. Indeed, we observe that the test statistics become negative even at shorter maturities (see the last three columns of Table 4). However, the results lose statistical significance because of the reduced sample size used in the test.

4.2 Probability distribution of future jump size

The 4F-model can be used to assess the probability distribution of rate changes after the next ECB meeting. The conditional distribution of the jump size is assumed to be normal with mean $\gamma \mathbb{E}_t[\xi_{T_J}]$ and variance $\gamma^2 \mathrm{Var}_t[\xi_{T_J}] + w^2$ where T_J is the date of a future possible jump. The mean and variance of the latent factor ξ_{T_J} are known in closed form and depend on the estimated values of the latent factors at time t. For representation purposes, we discretize the probability distribution by considering seven possible jump sizes ranging from -75 bps to 75 bps with increments of 25 bps.

Panel A: €STR

	All times			$\{\forall t : \exists T_J \text{ with } t < T_J < t + \tau\}$		
τ	4F RMSE	DNS RMSE	DM stat	4F RMSE	DNS RMSE	DM stat
10	22	12	9.55***	13	13	-0.06
20	19	15	5.17***	15	16	-1.25
30	17	19	-1.82*	17	19	-2.64***
60	25	30	-3.00***	25	30	-3.00***

Panel B: Euribor

10	20	12	8.74***	13	13	-0.84
20	18	15	4.05***	15	16	-1.01
30	17	18	-0.78	17	18	-1.14
60	25	28	-2.01**	25	28	-2.01**

Table 4: Forecast evaluation based on Diebold-Mariano test for different forecast horizons τ (in days). The table reports the root mean square errors (in basis points) for both the 4F-model and the benchmark model, as well as the Diebold-Mariano statistics. Negative values of the statistic indicate that the 4F-model outperforms the benchmark. The test is performed either considering all times t out-of-sample (left panel), or only those times t for which a jump occurs between t and the forecast horizon (right panel). Asterisks denote significance at the 10% (*), 5% (**), and 1% (***) levels.

Figure 8 displays the time series of probabilities of the next jump size. The vertical dashed lines correspond to the scheduled ECB meeting dates (i.e., potential jump times), and dots indicate the realized values. If a jump occurred of exactly -75, -50, -25, 0, 25, 50, or 75 basis points, the dot is placed in the corresponding probability region. For instance, on December 9, 2024, the estimated probabilities for the next expected jump on December 19 (i.e., 10 days later) were as follows: 10% for a -75 bps jump, 35% for -50 bps, 40% for -25 bps, and 15% for no jump. The realized jump was -25 basis points.

It is worth noting that, in market practice, a common approach to estimate the expected value of the upcoming jump in the policy rate is to compute the difference between the €STR-based OIS rate that starts on the date of the next ECB meeting and matures at the following one (i.e., covering the next maintenance period), and the prevailing overnight rate, such as the observed €STR. However, there is no standardized market methodology to estimate the full probability distribution of the jump size. Practitioners often rely on survey-based expectations, such as those published in the ECB Survey of Monetary Analysts, which reflect the average view of selected market participants. In this context, the model we propose offers a theoretically consistent and data-driven method for estimating not only the expected jump but also its entire conditional probability distribution.

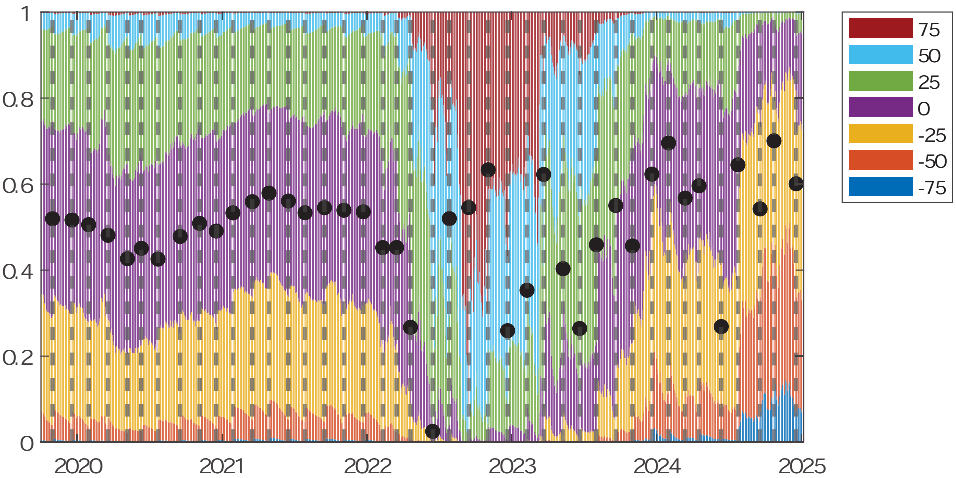

Figure 8: Time series of the estimated probability of the next jump size. Vertical dashed lines indicate times of potential jumps. Dots represent realized jumps. If a jump occurred at -75, -50, -25, 0, 25, 50, or 75 basis points, the dot is plotted in the probability region corresponding to that jump size.

4.3 Fallback risk

In the (not so unlikely) event that EURIBOR follows the destiny of the other "IBOR" rates and is discontinued, it will have to be replaced by a designated "fallback rate" in all derivative contracts referencing it, such as futures, swaps, caps, floors, and others. Currently, all new contracts written on EURIBOR are required to specify the fallback rate that will apply in the case of its discontinuation. The most common fallback rate is a term rate based on €STR. When market liquidity is sufficient, this fallback is typically the OIS rate. Otherwise, a fallback rate may be constructed using more liquid market instruments, as in the methodology proposed by Heitfield and Park (2019). We define the "fallback risk" as the risk that an EURIBOR based underlying is replaced by one related to €STR. With the model proposed in this paper, we can evaluate the financial risk of such a switch, conditional on the occurrence of a fallback event.

As an example, we consider a Forward Rate Agreement (FRA) where the floating leg is the EURIBOR settled at time T with maturity τ. If the EURIBOR is dismissed before time T, it must be replaced by a fallback rate. We assume that the fallback rate is the corresponding OIS written on €STR, that is, the τ maturity zero rate on €STR plus a credit spread adjustment δ.[1] Let F be the face value of the contract, then the loss for the leg of the contract that receives

[1] The credit spread adjustment is equal to the median of the differences between the old and the fallback rate in the five years preceding the trigger event. For example, it was set to 8.5 basis points when switching from EONIA to €STR.

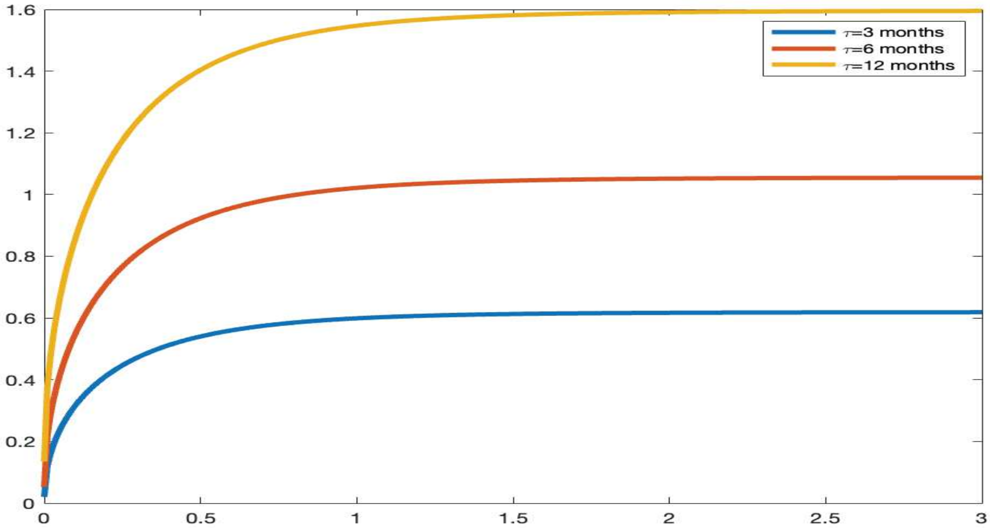

Figure 9: The 95% VaR, expressed as a percentage of the face value, in case of fallback of EURIBOR to €STR for FRA $T \times (T+\tau)$, as a function of T.

the floating payment at time T in case of fallback[2] is

$$L_T = \Big(y^{\text{EURIBOR}}(T, T+\tau) - y^{\text{€STR}}(T, T+\tau) - \delta \Big)\, \tau F.$$

The spread between the EURIBOR and the €STR rate is driven by the factor s_t. In particular, from Equation (4) we have

$$L_T = \big(\bar{A}(\tau) + \bar{B}(\tau) s_T - \delta \big)\, \tau F,$$

where

$$\begin{aligned} \bar{B}(\tau) &= \frac{-B(T, T+\tau)}{\tau} = \frac{1 - e^{-\kappa^s \tau}}{\kappa^s \tau} \\ \bar{A}(\tau) &= \frac{-A(T, T+\tau)}{\tau} = \left(\frac{\sigma^{s2}}{2\kappa^{s2}} - \bar{s} \right) \big(\bar{B}(\tau) - 1 \big) + \frac{\sigma^{s2}}{4\kappa^s} \bar{B}(\tau)^2 \tau \end{aligned}$$

because of Equation (11). Since the conditional distribution of the spread s_T is normal with mean (in the objective probability measure)

$$m(t, T) := s_t e^{-\kappa^s (T-t)} + (\bar{s} + \frac{\sigma^s \lambda^s}{k^s})(1 - e^{-\kappa^s (T-t)})$$

and variance

$$v(t, T) = \frac{\sigma^{s2}}{2\kappa^s} (1 - e^{-2\kappa^s (T-t)}),$$

[2]For simplicity, in this example we treat the continuously compounded rates like a simple rate.

we have

$$L_T \sim \left(\bar{A}(\tau) + \bar{B}(\tau)(m(t,T) + v(t,T)^{1/2}\epsilon) - \delta\right)\tau F,$$

with ϵ a standard normal variable, that is, L_T is a normal random variable with mean

$$M_L(t,T) = (\bar{A}(\tau) + \bar{B}(\tau)m(t,T) - \delta)\tau F$$

and variance

$$V_L(t,T) = \bar{B}(\tau)^2 v(t,T)\tau^2 F^2.$$

Figure 9 shows an application of these results to the computation of the 95% Value at Risk (VaR) as a function of T and for τ equal to 3, 6, and 12 months. To produce the plot we took as the evaluation time the last date of our data set (January 6, 2025) and we set the credit spread δ to zero. We note that VaR increases with T and approaches a constant value for T greater than 1.5 years because of the effect of mean reversion. The VaR reaches a level of about 1% of the face value for the 6 month FRA and it increases with the length of the time interval τ.

4.4 Sensitivity of the yields to changes in the expected short term rate

An important issue in monetary policy is to assess the sensitivity of the term structure to changes in the expected level of the rates fixed by the central bank. More precisely, it is highly relevant to quantify how a variation in the expected value of the next jump affects the expected yields across different maturities. Our model allows for the computation of this quantity.

Let us denote by $F_t := E_t[J_{T_1}]$ the conditional expectation of the change in the short term rate at the next jump day $T_1 > t$. The variation of F_t from t to $t+h$ is

$$\Delta_h F_t := F_{t+h} - F_t$$

and the variation in the yield is

$$\Delta_h y(t,T) := y(t,T) - y(t+h, T+h).$$

We want to compute the expectation of the yield variation $\Delta_h y(t,T)$, conditioned on the change $\Delta_h F_t$ in the expectation of the next possible jump. Since $\Delta_h y(t,T)$ and $\Delta_h F_t$ are jointly gaussian, such a quantity is

$$E_t[\Delta_h y(t,T)|\Delta_h F_t] = E_t[\Delta_h y(t,T)] + \frac{\mathrm{Cov}_t[\Delta_h y(t,T), \Delta_h F_t]}{\mathrm{Var}_t[\Delta_h F_t]}\Delta_h F_t. \tag{15}$$

The different contributions in (15) are reported in Appendix A.3.

We apply Formula (15) to compute the variation in the term structure of the €STR zero rates on September 18, 2020, resulting from changes in the expectation of the next possible jump (occurring on November 5, 2020) equal to $-5, 5, 10$ basis points. We set the time horizon h equal to 3 days. The results are displayed in Figure 10. We see that maturities up to 1 month are not affected by the change because the next jump time occurs afterwards. The impact of the changes in the expectation of the next jump size has a humped shape. This is because the effect of the changes increases with maturity up to 2 years. This can be explained by the fact that market traders expect central banks to move the interest rates gradually, with a strategy called *inertia*, where a series of small moves of the interest rate usually take place rather than a big sudden movement. The interest rates are then expected to revert to the previous levels, and this produces the humped shape of the sensitivity.

By comparing Figure 10 with Figure 7, we observe that a variation in the term structure of the order of magnitude of the sample standard deviation of the term structure in the "no-jump" case may be obtained by a change in the expected jump size of the short-term rate at the next jump date of less than 5 basis points.

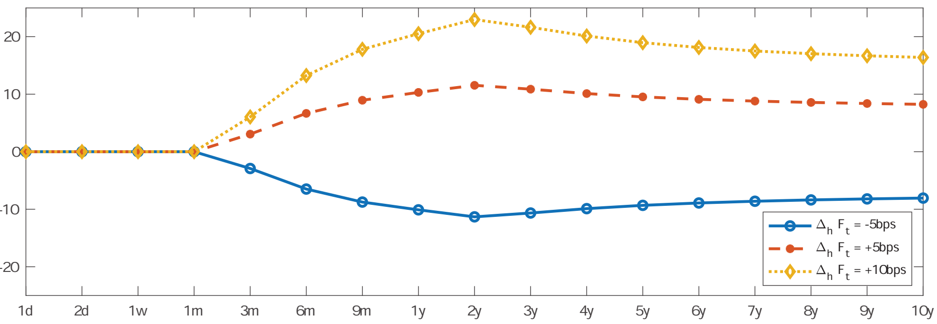

Figure 10: Expected yield variations induced by a variation $\Delta_h F_t$ of the expected jump size at the next jump time, for three values of $\Delta_h F_t$. The plot is obtained from Formula (15) for t equal to September 18, 2020. The next possible jump date is November 5, 2020. We set the time shift h equal to 3 days.

5 Conclusion

We proposed a four-factor affine term structure model designed to jointly capture the dynamics of EURIBOR- and €STR-based term structures in the post-LIBOR world. The model incorporates the possibility of scheduled jumps in the short rate process within an affine framework. These jumps are aligned with ECB policy meeting dates, thereby capturing the impact of monetary policy decisions on yields across different maturities. The model outperforms the widely used Dynamic Nelson-Siegel benchmark, both in-sample and out-of-sample, despite relying on fewer parameters, highlighting the relevance of incorporating policy-driven discontinuities into interest rate modeling.

Beyond its statistical accuracy in fitting the observed term structures, we illustrated several relevant applications that leverage its key features. These include forecasting future term structures, computing the probability distribution of upcoming policy-induced jumps, assessing fallback risk in derivatives linked to EURIBOR, and analyzing the sensitivity of interest rate curves to shifts in monetary policy expectations. The model offers a robust and parsimonious tool for central banks, risk managers, and financial market participants.

A Appendix

A.1 Proof of Proposition 1

The proof follows the same lines as that of Proposition 1 in Kim and Wright (2014) and we report it for the convenience of the reader.

At time t, consider a zero-coupon bond with maturity T. Its price can be computed as

$$P^{€STR}(t,T) = \mathbb{E}_t^Q\left[e^{-\int_t^T r_u du}\right] = \mathbb{E}_t^Q\left[e^{-\int_t^T \left(r_t + \sum_{i=1}^n J_{T_i}\right)du}\right] = \\ = e^{-r_t(T-t)}\mathbb{E}_t^Q\left[e^{-\sum_{i=1}^n J_{T_i}(T-T_i)}\right], \tag{16}$$

where, recall, $T_i \in \mathcal{T}$ is a time of possible jump, for $i = 1, 2, \ldots, n$, and $t \leq T_1 < T_2 < \ldots < T_n < T$. Whenever $n \geq 1$, we compute the expectation in (16) with a backward recursion using the law of iterated expectations. To do so, for any k, $1 \leq k \leq n$, let us define $G(T_k, \ldots, T_n, T)$ and the D-vector $F(T_k, \ldots, T_n, T)$ such that

$$\mathbb{E}_{T_k}^Q\left[e^{-\sum_{i=k}^n J_{T_i}(T-T_i)}\right] = e^{G(T_k \ldots, T_n, T) + F(T_k, \ldots, T_n, T)' X_{T_k}}. \tag{17}$$

First of all we have

$$\mathbb{E}_{T_n}^Q\left[e^{-J_{T_n}(T-T_n)}\right] = e^{-(T-T_n)a' X_{T_n} + \frac{1}{2}w^2(T-T_n)^2}.$$

Hence,

$$G(T_n, T) = \frac{1}{2}w^2(T-T_n)^2, \tag{18}$$

$$F(T_n, T) = -(T-T_n)a. \tag{19}$$

Now we apply the law of iterated expectations to the left-hand side of (17) to find a recursive relation:

$$\mathbb{E}_{T_k}^Q\left[e^{-\sum_{i=k}^n J_{T_i}(T-T_i)}\right] = \mathbb{E}_{T_k}^Q\left[e^{-J_{T_k}(T-T_k)}\mathbb{E}_{T_{k+1}}^Q\left[e^{-\sum_{i=k+1}^n J_{T_i}(T-T_i)}\right]\right] = \\ = e^{-(T-T_k)a' X_{T_k -} + \frac{1}{2}w^2(T-T_k)^2}\mathbb{E}_{T_k}^Q\left[e^{G(T_{k+1}, \ldots, T_n, T) + F(T_{k+1}, \ldots, T_n, T)' X_{T_{k+1}}}\right] = \\ = e^{-(T-T_k)a' X_{T_k} + \frac{1}{2}w^2(T-T_k)^2 + G(T_{k+1}, \ldots, T_n, T)}\mathbb{E}_{T_k}^Q\left[e^{F(T_{k+1}, \ldots, T_n, T)' X_{T_{k+1}}}\right]. \tag{20}$$

The last expected value is the moment generating function of the process X_t. From Equation (2), we have

$$\mathbb{E}_{T_k}^Q\left[e^{F(T_{k+1}, \ldots, T_n, T)' X_{T_{k+1}}}\right] = \\ = e^{\Phi^Q(T_{k+1}-T_k, F(T_{k+1}, \ldots, T_n, T)) + \Psi^Q(T_{k+1}-T_k, F(T_{k+1}, \ldots, T_n, T))' X_{T_k}}.$$

Equation (20) can then be written as

$$\mathbb{E}_{T_k}^Q\left[e^{-\sum_{i=k}^n J_{T_i}(T-T_i)}\right] = e^{-(T-T_k)a' X_{T_k} + \frac{1}{2}w^2(T-T_k)^2 + G(T_{k+1}, \ldots, T_n, T)} \\ \times e^{\Phi^Q(T_{k+1}-T_k, F(T_{k+1}, \ldots, T_n, T)) + \Psi^Q(T_{k+1}-T_k, F(T_{k+1}, \ldots, T_n, T))' X_{T_k}}. \tag{21}$$

Combining Equation (17) and Equation (21), we find backward recursive relations

$$\begin{aligned}G(T_k,\ldots,T_n,T) &= \frac{1}{2}w^2(T-T_k)^2 + G(T_{k+1},\ldots,T_n,T)+\\ &\quad + \Phi^Q(T_{k+1}-T_k, F(T_{k+1},\ldots,T_n,T)),\\ F(T_k,\ldots,T_n,T) &= -(T-T_k)a + \Psi^Q(T_{k+1}-T_k, F(T_{k+1},\ldots,T_n,T)).\end{aligned}$$

Starting from (18) and (19) and following the backward recursions, it is possible to obtain $G(T_1,\ldots,T_n,T)$ and $F(T_1,\ldots,T_n,T)$. In conclusion, the price of a zero-coupon bond (16) is

$$\begin{aligned}P^{€STR}(t,T) &= e^{-r_t(T-t)}\mathbb{E}_t^Q\left[e^{G(T_1,\ldots,T_n,T)+F(T_1,\ldots,T_n,T)'X_{T_1}}\right]\\ &= e^{-r_t(T-t)+G(T_1,\ldots,T_n,T)+\Phi^Q(T_1-t,F(T_1,\ldots,T_n,T))+\Psi^Q(T_1-t,F(T_1,\ldots,T_n,T))'X_t}\end{aligned}$$

and the corresponding zero-coupon yield on €STR is

$$\begin{aligned}y^{€STR}(t,T) &= r_t - \frac{1}{T-t}\big(G(T_1,\ldots,T_n,T) + \Phi^Q(T_1-t, F(T_1,\ldots,T_n,T))\big)\\ &\quad - \frac{1}{T-t}\Psi^Q(T_1-t,F(T_1,\ldots,T_n,T))'X_t.\end{aligned}$$

which is Equation (3) in Proposition 1.

A.2 State-space formulation and the Kalman filter

To calibrate the model, we employ the Kalman filter. First, we express the model in an equivalent state-space formulation. At times $t_1,\cdots,t_{N_{obs}}$ we observe yields on €STR and EURIBOR with time to maturities $\tau_1,\cdots,\tau_N$. Then, the $2N$-vector of observables at time t_i, for $i=1,\cdots,N_{obs}$, is

$$y_i = \begin{pmatrix} y^{€STR}(t_i,t_i+\tau_1)\\ \vdots\\ y^{€STR}(t_i,t_i+\tau_N)\\ y^{EURIBOR}(t_i,t_i+\tau_1)\\ \vdots\\ y^{EURIBOR}(t_i,t_i+\tau_N)\end{pmatrix}.$$

We define the $(D+2)$-vector of latent factors at time t_i, $i=1,\cdots,N_{obs}$, as

$$\alpha_i = \begin{pmatrix} X_{t_i}\\ r_{t_i}\\ s_{t_i}\end{pmatrix}.$$

The measurement equation

$$y_i = d_i + Z_i\alpha_i + \Sigma_i\epsilon_i, \qquad i=1,\ldots,N_{obs} \tag{22}$$

follows from Equations (3-4). For any t and any $T > t$, we introduce a simplified notation for the functions in Equation (3) of Proposition 1:

$$\begin{aligned} g(t,T) &\coloneqq G(T_1,\dots,T_n,T) \\ f(t,T) &\coloneqq F(T_1,\dots,T_n,T), \end{aligned}$$

by dropping the dependence on jump times between t and T, and explicitly writing the evaluation time t. We also set $g(t,T) = f(t,T) = 0$ in the event there are no jumps between t and T. With that notation, we have

$$d_i = \begin{pmatrix} -\frac{1}{\tau_1}\left(g(t_i,t_i+\tau_1) + \Phi^Q(T_1-t_i, f(t_i,t_i+\tau_1))\right) \\ \vdots \\ -\frac{1}{\tau_N}\left(g(t_i,t_i+\tau_N) + \Phi^Q(T_1-t_i, f(t_i,t_i+\tau_N))\right) \\ -\frac{1}{\tau_1}\left(g(t_i,t_i+\tau_1) + \Phi^Q(T_1-t_i, f(t_i,t_i+\tau_1)\right) + A(t_i,t_i+\tau_1)) \\ \vdots \\ -\frac{1}{\tau_N}\left(g(t_i,t_i+\tau_N) + \Phi^Q(T_1-t_i, f(t_i,t_i+\tau_N)\right) + A(t_i,t_i+\tau_N)) \end{pmatrix},$$

$$Z_i = \begin{pmatrix} -\frac{1}{\tau_1}\Psi^Q(T_1-t_i, f(t_i,t_i+\tau_1))' & 1 & 0 \\ \vdots & \vdots & \vdots \\ -\frac{1}{\tau_N}\Psi^Q(T_1-t_i, f(t_i,t_i+\tau_N))' & 1 & 0 \\ -\frac{1}{\tau_1}\Psi^Q(T_1-t_i, f(t_i,t_i+\tau_1))' & 1 & -\frac{1}{\tau_1}B(t_i,t_i+\tau_1) \\ \vdots & \vdots & \vdots \\ -\frac{1}{\tau_N}\Psi^Q(T_1-t_i, f(t_i,t_i+\tau_N))' & 1 & -\frac{1}{\tau_N}B(t_i,t_i+\tau_N) \end{pmatrix},$$

ϵ_i is a $(2N + D + 2) \times 1$ vector of normal iid errors,

$$\Sigma_i = \begin{pmatrix} \sigma I_{2N\times 2N} & 0_{2N\times(D+2)} \end{pmatrix}$$

where $I_{2N\times 2N}$ is the identity matrix and σ is the measurement error that we assume to be the same across the different time series used for filtering.

The vector of latent factors α follows an affine process under the objective probability measure. Hence, we can compute its conditional mean and variance and, following Filipović and Trolle (2013), approximate the transition density with a Gaussian distribution that shares the same first and second moments.[3] Therefore the transition equation reads as follows

$$\alpha_{i+1} = M_i\alpha_i + c_i + \Omega_i\epsilon_i \qquad i = 1,\cdots,N_{obs} \tag{23}$$

where M_i is the $(D + 2) \times (D + 2)$ transition matrix

$$M_i = \begin{pmatrix} \nabla_u \Psi'(t_{i+1}-t_i,u)\big|_{u=0} & 0_{D\times 1} & 0_{D\times 1} \\ \mathbf{1}_{t_i\in\mathcal{T}}a' & 1 & 0 \\ 0_{1\times D} & 0 & \frac{d\Psi_s(t_{i+1}-t_i,v)}{dv}\Big|_{v=0} \end{pmatrix},$$

[3]We remark that the transition density is indeed Gaussian under the specific model introduced in Section 3.2, which is used for calibration and application purposes.

with $\nabla_u \Psi'$ being the Jacobian matrix of Ψ with respect to u,

$$c_i = \begin{pmatrix} \nabla_u \Phi(t_{i+1} - t_i, u)|_{u=0} \\ 0 \\ \left.\frac{d\Phi_s(t_{i+1}-t_i,v)}{dv}\right|_{v=0} \end{pmatrix},$$

and

$$\Omega_i = \begin{pmatrix} 0_{D\times N} & h_i & 0_{D\times 1} & 0_{D\times 1} \\ 0_{1\times N} & 0_{1\times D} & w\mathbf{1}_{t_i\in\mathcal{T}} & 0 \\ 0_{1\times N} & 0_{1\times D} & 0 & \sqrt{\left.\frac{d^2\Phi_s(t_{i+1}-t_i,v)}{dv^2}\right|_{v=0}} \end{pmatrix},$$

with h_i a lower triangular matrix such that $h_i h_i' = H_u \Phi(t_{i+1} - t_i, u)|_{u=0}$, and $H_u\Phi$ being the hessian matrix of Φ with respect to u.

The Kalman filter is obtained by solving the following recursion equations. First, we define the conditional expectation and the covariance matrix for the state variables

$$\begin{aligned} \tilde{\alpha}_{i|i-1} &= \mathbb{E}[\alpha_i|\mathcal{F}_{i-1}] \\ P_{i|i-1} &= \mathrm{Cov}[\alpha_i|\mathcal{F}_{i-1}] \end{aligned}$$

where $\mathcal{F}_{i-1}$ is the information given by the observation of yields up to time t_{i-1}, for $i = 1, \ldots, N_{obs}$. The innovation process, defined as the one-step ahead prediction error, is

$$\begin{aligned} \nu_i &= y_i - Z_i \tilde{\alpha}_{i|i-1} - d_i \\ &= y_i - \mathbb{E}[y_i|\mathcal{F}_{i-1}] \end{aligned}$$

with covariance matrix

$$\Sigma_i^\nu = Z_i P_{i|i-1} Z_i' + \Sigma_i \Sigma_i'.$$

Then, the update equations for the filter are

$$\begin{aligned} \tilde{\alpha}_{i+1|i} &= c_i + M_i \tilde{\alpha}_{i|i-1} + K_i \nu_i \\ P_{i+1|i} &= M_i P_{i|i-1} M_i' + \Omega_i \Omega_i' - K_i \Sigma_i^\nu K_i' \end{aligned}$$

where

$$K_i = M_i P_{i|i-1} Z_i' (\Sigma_i^\nu)^{-1}.$$

The recursion starts with an initial point. We assume that $\alpha_1 \sim \mathcal{N}(\tilde{\alpha}_{1|0}, P_{1|0})$, where $\tilde{\alpha}_{1|0}$ and $P_{1|0}$ are set to the stationary state. The model can be calibrated by maximizing the log likelihood

$$\mathcal{L}(y_1, \ldots, y_{N_{obs}}; \theta) = -\frac{1}{2} \left(\sum_{i=1}^{N_{obs}} \ln \det(\Sigma_i^\nu) + \sum_{i=1}^{N_{obs}} \nu_i' (\Sigma_i^\nu)^{-1} \nu_i \right)$$

where θ is the vector of model parameters.

A.3 Useful formulas

In this subsection we provide the necessary tools for the computations of the unconditional variance of the €STR-based yield term structure as in Equation (8) and for the sensitivity of the term structure to changes on the expectation of the short term rates in Formula (15).

Le us consider the dynamics of $X_t = (\xi_t, \theta_t)'$ in matrix form (14). The process X_t satisfies

$$X_{t+h} = \Lambda(h)X_t + \mu(h) + \varepsilon(h)$$

where $\varepsilon(\ell) \sim \mathcal{N}(0, Q(\ell))$, $\Lambda(\ell) = e^{-K\ell}$, $\mu(\ell) = \int_0^\ell e^{-K's} K\bar{X}\, ds$, $Q(\ell) = \int_0^\ell e^{-Ks}\Sigma_X\Sigma_X' e^{-K's}\, ds$. Hence,

$$\Delta_h X_t = (\Lambda(h) - I)X_t + \mu(h) + \varepsilon(h),$$

where I is the identity matrix of conformable dimension. The stationary variance of X_t is

$$\mathrm{Var}[X_t] = S$$

where S is the solution to the Lyapunov Equation:

$$KS + SK' = \Sigma_X\Sigma_X'.$$

In the following we assume that X_t has reached the stationary distribution.

The other quantities necessary to compute (8) are

$$\begin{aligned} \mathrm{Cov}[X_t, \Delta_h X_t] &= S(\Lambda(h) - I)' \\ \mathrm{Var}[\Delta_h X_t] &= (\Lambda(h) - I)S(\Lambda(h) - I)' + Q(h) \\ \mathrm{Cov}[X_t, X_{T_J}] &= S\Lambda(T_J - t)' \end{aligned}$$

and

$$\begin{aligned} \mathrm{Cov}[\Delta_h X_t, X_{T_J}] &= \mathrm{Cov}[X_{t+h} - X_t, X_{T_J}] \\ &= \mathrm{Cov}[X_{t+h}, X_{T_J}] - \mathrm{Cov}[X_t, X_{T_J}] \\ &= \Lambda(t + h - T_J)S - S\Lambda(T_J - t)'. \end{aligned}$$

To compute Formula (15) we start from Equation (6) for $\Delta_h y(t, T)$, where we take into account that $T_j > t + h$

$$\Delta_h y(t, T) = \Delta_h d^X + C'X_t + D'\Delta_h X_t. \tag{24}$$

For Formula (15) we need

$$E_t[\Delta_h y(t, T)] = \Delta_h d^X + C'X_t + D'E_t[\Delta_h X_t]$$

where

$$E_t[\Delta_h X_t] = (\Lambda(h) - I)X_t + \mu(h).$$

Moreover,

$$\begin{aligned}
\Delta_h F_t &= E_{t+h}[J_{T_1}] - E_t[J_{T_1}] \\
&= a' E_{t+h}[X_{T_1}] - a' E_t[X_{T_1}] \\
&= a' \left(\Lambda(T_1 - (t+h)) X_{t+h} - \Lambda(T_1 - t) X_t + \mu(T_1 - (t+h)) - \mu(T_1 - t) \right).
\end{aligned}$$

Hence,

$$\begin{aligned}
\mathrm{Cov}_t[\Delta_h y(t,T), \Delta_h F_t] &= \mathrm{Cov}_t[D' \Delta_h X_t, a' \left(\Lambda(T_1 - (t+h)) X_{t+h} - \Lambda(T_1 - t) X_t \right)] \\
&= D' \mathrm{Cov}_t[\Delta_h X_t, X_{t+h}] \Lambda(T_1 - (t+h))' a \\
&= D' \mathrm{Var}_t[X_{t+h}] \Lambda(T_1 - (t+h))' a \\
&= D' Q(h) \Lambda(T_1 - (t+h))' a
\end{aligned}$$

and

$$\begin{aligned}
\mathrm{Var}_t[\Delta_h F_t] &= a' \Lambda(T_1 - (t+h)) \mathrm{Var}_t[X_{t+h}] \Lambda(T_1 - (t+h))' a \\
&= a' \Lambda(T_1 - (t+h)) Q(h) \Lambda(T_1 - (t+h))' a.
\end{aligned}$$

References

Backwell, A. and Hayes, J. (2022). Expected and unexpected jumps in the overnight rate: Consistent management of the libor transition. *Journal of Banking & Finance*, 145:106669.

BIS (2019). Beyond libor: A primer on the new benchmark rates.

Brace, A., Gellert, K., and Schlögl, E. (2024). Sofr term structure dynamics-discontinuous short rates and stochastic volatility forward rates. *Journal of Futures Markets*, 44(6):936–985.

Calvia, A., De Donno, M., Guardasoni, C., and Sanfelici, S. (2025). Short-rate models with stochastic discontinuities: a pde approach. *Working paper*.

Diebold, F. and Mariano, R. (1995). Comparing predictive accuracy. *Journal of Business & Economic Statistics*, 13:253–263.

Diebold, F. X., Rudebusch, G. D., and Aruoba, S. B. (2006). The macroeconomy and the yield curve: a dynamic latent factor approach. *Journal of econometrics*, 131(1-2):309–338.

ECB (2021). On euribor fallback trigger events and €str-based euribor fallback rates.

ECB (2025). Euro money market study 2024.

Filipović, D. and Trolle, A. B. (2013). The term structure of interbank risk. *Journal of Financial Economics*, 109(3):707–733.

Fontana, C. (2023). Caplet pricing in affine models for alternative risk-free rates. *SIAM Journal on Financial Mathematics*, 14(1):SC1–SC16.

Fontana, C., Grbac, Z., Gümbel, S., and Schmidt, T. (2020). Term structure modelling for multiple curves with stochastic discontinuities. *Finance and Stochastics*, 24(2):465–511.

Fontana, C., Grbac, Z., and Schmidt, T. (2024). Term structure modeling with overnight rates beyond stochastic continuity. *Mathematical Finance*, 34(1):151–189.

Gellert, K. and Schlögl, E. (2021). Short rate dynamics: A fed funds and sofr perspective. *arXiv preprint arXiv:2101.04308*.

Heitfield, E. and Park, Y.-H. (2019). Inferring term rates from sofr futures prices. *Finance and Economics Discussion Series 2019-014. Washington: Board of Governors of the Federal Reserve System*.

ICMA (2023). Benchmark reform and transition to risk-free rates.

ISDA (2023). Progress on global transition to rfrs in derivatives markets.

Jermann, U. (2024). Interest received by banks during the financial crisis: Libor vs hypothetical sofr loans. *Journal of Financial Services Research*, 65(2):141–152.

Kim, D. H. and Wright, J. H. (2014). Jumps in bond yields at known times.

Kirti, D. (2022). What are reference rates for? *Journal of Banking & Finance*, 144:106635.

Klingler, S. and Syrstad, O. (2021). Life after libor. *Journal of Financial Economics*, 141(2):783–801.

Nelson, C. R. and Siegel, A. F. (1987). Parsimonious modeling of yield curves. *Journal of business*, pages 473–489.

Piazzesi, M. (2001). An econometric model of the yield curve with macroeconomic jump effects. *National Bureau of Economic Research Cambridge, Mass., USA*. `https://www.nber.org/papers/w8246`.

Piazzesi, M. (2005). Bond yields and the federal reserve. *Journal of Political Economy*, 113(2):311–344.

Piazzesi, M. (2010). Affine term structure models. In *Handbook of financial econometrics: Tools and Techniques*, pages 691–766. Elsevier.

Schlögl, E., Skov, J. B., and Skovmand, D. (2023). Term structure modeling of sofr: Evaluating the importance of scheduled jumps. *Available at SSRN 4431839*.

Skov, J. B. and Skovmand, D. (2021). Dynamic term structure models for sofr futures. *Journal of Futures Markets*, 41(10):1520–1544.

Skov, J. B. and Skovmand, D. (2023). Decomposing libor in transition: evidence from the futures markets. *Quantitative Finance*, 23(6):959–978.

RECENT PUBLICATIONS BY *CEIS Tor Vergata*

From Knowledge to Allocation of Sustainable Assets: Results From An In-Field Survey In Italy
Beatrice Bertelli, Marianna Brunetti, Costanza Torricelli, Mariangela Zoli
CEIS *Research Paper*, 612 October 2025

VAR Models With An Index Structure: A Survey With New Results
Gianluca Cubadda
CEIS *Research Paper*, 611 September 2025

Beyond Colors: Communication and Social Identity in Natural Groups
Giovanni Di Bartolomeo, Stefano Papa and Alessandra Pelloni
CEIS *Research Paper*, 610 September 2025

Technology Spillovers from the Final Frontier: A Long-Run View of U.S. Space Innovation
Luisa Corrado, Stefano Grassi and Aldo Paolillo
CEIS *Research Paper*, 609 August 2025

Identification, Estimation and Inference in High-Frequency Event Study Regressions
Alessandro Casini and Adam McCloskey
CEIS *Research Paper*, 608 July 2025

When Fewer Bids Increase Competition: Buyer Surplus Enhancing Mergers in Single-Award Procurement Auctions
Gian Luigi Albano, Walter Ferrarese and Roberto Pezzuto
CEIS *Research Paper*, 607 July 2025

The State-Dependent Consumption Response to Government Spending in US: a Markov-Switching TANK Model with Sticky Wages
Francesco Morelli
CEIS *Research Paper*, 606 June 2025

Catastrophic Risk Perception and the Shared Burden Effect: An Experimental Study Using Prospect Theory
Riccardo Manghi and Daniela Di Cagno
CEIS *Research Paper*, 605 June 2025

New Keynesian Models, Puzzles and Omitted Effects
Francesco Morelli
CEIS *Research Paper*, 604 June 2025

A Foundation for Universalisation in Games
Enrico Mattia Salonia
CEIS *Research Paper*, 603 June 2025